Thermodynamics and Kinetics of the Gas-Phase Reactions: $H_3O^+(H_2O)_{n-1} + H_2O = H_3O^+(H_2O)_n$

Y. K. Lau, S. Ikuta, and P. Kebarle*

Contribution from the Chemistry Department, University of Alberta, Edmonton, Alberta, Canada T6G 2G2. *Received August 14, 1981*

Abstract: The temperature dependence of equilibrium constants $K_{n-1,n}$ for reactions $H_3O^+(H_2O)_{n-1} + H_2O = H_3O^+(H_2O)_n$ was determined in a pulsed electron beam high ion source pressure mass spectrometer. Methane was used as a major gas. van't Hoff plots over a wide temperature range could be obtained. The new determinations lead to $\Delta G°_{n-1,n}$, $\Delta H°_{n-1,n}$, and $\Delta S°_{n-1,n}$ which are fairly close to those obtained in earlier measurements from this laboratory. However, the $-\Delta H°$ (3,4), (4,5), and (5,6) are lower than those observed previously. This result gives greater prominence to the stability of the $H_3O^+(H_2O)_3$ structure. The trends predicted by the $\Delta H°_{n-1,n}$ of the present data are very similar to those obtained by 4-31G molecular orbital calculation by M. D. Newton. The third-order rate constants k_n for the forward reactions $(n-1,n)$ were determined over a wide temperature range. The rate constants follow the empirical relationship $k = aT^{-b}$. The changes with n show a certain regularity; thus both a and b increase with n. However, the increase is not continuous but follows the trends observed for the equilibrium constants $K_{n-1,n}$; i.e., there are larger changes after (0,1) and (2,3) which reflect the changes of stabilities of the hydrates n. Changes of the rate constants k_n for the potassium hydrates $K^+(H_2O)_n$ predicted by theory are much more regular, reflecting the gradual changes in the potassium hydrates. Some studies of the collision-induced decomposition (CID) were made by measuring the metastables $H_3O^+(H_2O)_n \rightarrow H_3O^+(H_2O)_{n-1}$ resulting from introduction of methane in the mass analysis system. It was found that the CID cross sections increase rapidly with n. This is attributed to the decreasing dissociation energies $\Delta H°_{n,n-1}$. The CID cross sections were found to increase with the temperature of the ion source, i.e., with the internal energy of the $H_3O^+(H_2O)_n$. Appreciable CID decomposition occurs already at mass analysis tube pressures of 10^{-6} Torr.

Introduction

The hydration reactions in eq 1 occur in nature, i.e., the earth's

$$H_3O^+(H_2O)_{n-1} + H_2O = H_3O^+(H_2O)_n \qquad (1)$$

atmosphere, and also under many experimental conditions. Therefore, data on the kinetics and equilibria of these reactions are useful to fields like ion chemistry of the ionosphere,[1] atmospheric electrocity,[2] electrical conductivity of air and electric discharges,[3] early phases of nucleation,[4] flames,[5] and radiation chemistry. Recent work even claims the involvement of reactions 1 in the formation of warm water fogs and the atmospheric infrared continuum absorption.[6]

The clustering of molecules around ions provides also information on the strong (inner shell) solvation of ions.[7] The thermodynamic data, i.e., $\Delta G°_{n-1,n}$, $\Delta H°_{n-1,n}$, and $\Delta S°_{n-1,n}$, obtained from measured temperature dependence of equilibrium constants $K_{n-1,n}$ are of interest to the field of ion solvation in condensed media[7] and theoretical attempts to describe this solvation by quantum mechanical calculation of the binding of a few solvent molecules to the ion[8,9] and extended statistical calculations.[9]

Experimental determinations of the temperature dependence of the equilibria 1 leading to the mentioned thermodynamic data have been published from this[10,11] and other laboratories.[12] However, only the temperature dependence of the rate constant k_1 for the reaction (0,1) has been studied.[11,12] Only a few isolated determinations,[13,14] mostly at room temperature, for some of the rate constants of the subsequent clustering reactions have been made.[13,14] A sequence of reactions $(n-1,n)$ may be expected to lead to a pattern of regular changes of the corresponding rate constants k_n, yet such a pattern has not been described for any given clustering system. The pattern can be obtained only from measurement of the temperature dependence of the rate constants. The present work provides such determinations. These results are of significance also to the development of ion molecule kinetics theory.

The main impetus toward the present measurements came from our recent concern[15] that some of the measurements of the equilibrium constants for the higher $(n-1,n)$ equilibria may be leading to $-\Delta H°_{n-1,n}$ and $\Delta S°_{n-1,n}$ results which are higher than the true values. An analysis[15] of the potassium ion hydrates $K^+(H_2O)_n$ indicated that for the higher clusters with $n > 4$ measurements in which neat water vapor was used in the ion source lead to conditions where a significant fraction of the clusters n participating in the equilibrium $(n-1,n)$ may be excited above the dissociation limit $(\Delta H°_{n,n-1})$. These energized clusters can dissociate in the vacuum of the mass analysis system.[15] The problem can be minimized by working with a mixture consisting of a major gas, e.g., methane, containing a small amount of water vapor. The forward clustering rates under these conditions are much slower, and this permits measurement of the equilibrium $(n-1,n)$ at much lower temperatures.

The hydronium ion equilibria (0,1), (1,2), and (2,3) were measured with methane as the major gas (Cunningham[11]), but the higher equilibria had been determined in earlier work[10] with neat water in the Torr range. Therefore, a redetermination of these equilibria under proper conditions was deemed necessary.

The decomposition of ion clusters in the vacuum of the mass spectrometer can be studied by detecting the "metastable" ions resulting from the decomposition $n \rightarrow n-1$ which occurs in the mass spectrometer analyzer tube. If one wishes to distinguish between true unimolecular decomposition of the energized ions

(1) Narcisi, R. S.; Bailey, A. D. *J. Geophys. Rev.* **1965**, *70*, 3687. Fehsenfeld, F. C.; Ferguson, E. E. *J. Geophys. Rev. Space Phys.* **1969**, *74*, 2217.
(2) Palmer, J. A. "Atmospheric Electricity"; Pergamon Press: New York, 1967.
(3) Lindinger, W. *Phys. Rev. A* **1973**, *7*, 328.
(4) Castleman, A. W., Jr. *Adv. Colloid Interface Sci.* **1979**, *10*, 73.
(5) Knewstubb, P. F.; Sugden, T. M. *Proc. R. Soc. London, Ser. A* **1960**, *225*, 520.
(6) Carlon, H. R.; Harden, C. S. *Appl. Opt.* **1980**, *19*, 1776.
(7) Kebarle, P. In "Modern Aspects of Electrochemistry"; Conway, B. E., Bockris, J. O'M., Ed.; Plenum Press: New York, 1974; Vol. 9.
(8) Diercksen, G. H. F.; Kraemer, W. P. *Thoer. Chim. Acta* **1972**, *23*, 387, 393.
(9) Clementi, E. "Lecture Notes in Chemistry"; Springer Verlag: New York, 1976; Vol. 2.
(10) Kebarle,, P.; Searles, S. K.; Zolla, A.; Scarborough, J.; Arshadi, M. *J. Am. Chem. Soc.* **1967**, *89*, 6393.
(11) Cunningham, A. J.; Payzant, J. D.; Kebarle, P. *J. Am. Chem. Soc.* **1972**, *94*, 7627.
(12) Meot-Ner, M.; Field, F. H. *J. Am. Chem. Soc.* **1977**, *99*, 998. Field, F. H. *Ibid.* **1969**, *91*, 2827.
(13) Good, A.; Durden, D. A.; Kebarle, P. *J. Chem. Phys.* **1970**, *52*, 222.
(14) Young, C. D.; Edelson, D.; Falconer, W. E. *J. Chem. Phys.* **1970**, *53*, 4295.
(15) Sunner, J.; Kebarle, P. *J. Phys. Chem.* **1981**, *85*, 327.

0002-7863/82/1504-1462$01.25/0

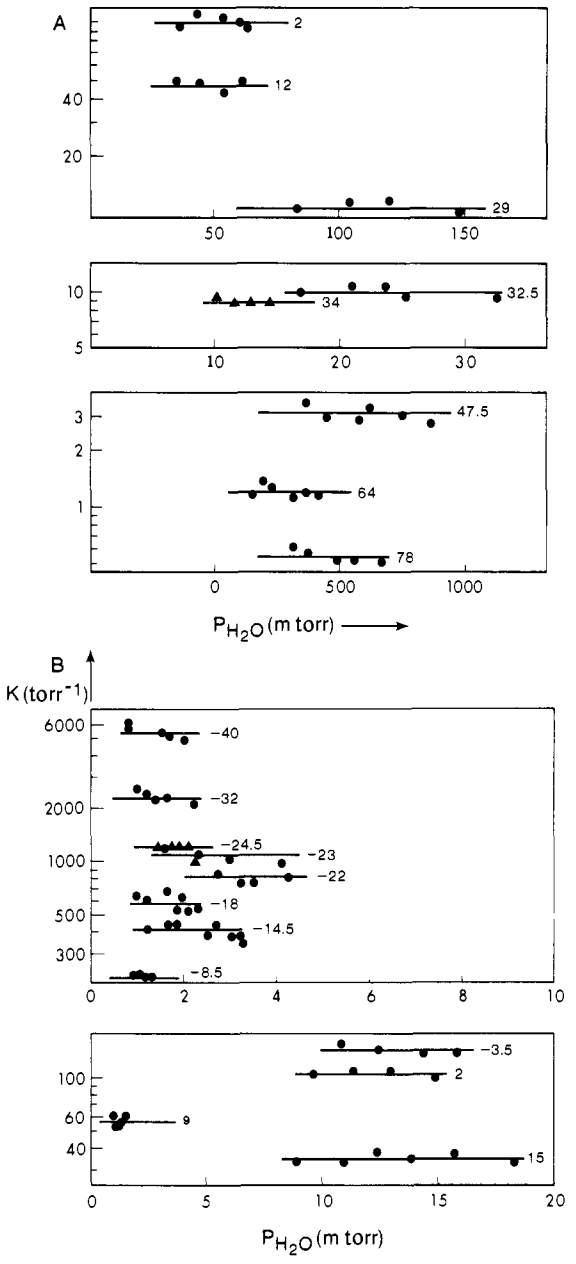

Figure 1. (*A*,*B*) Measured equilibrium constant $K = K_{3,4}$ for the equilibrium $H_3O^+(H_2O)_3 + H_2O = H_3O^+(H_2O)_4$. Mixtures of the major gas methane containing the partial pressures of water shown on the abscissa were used. The points for one given determination in the figure were generally obtained by using a constant methane to water ratio and changing the total ion source pressure. The water partial pressure range shown in the figure generally corresponds to a total ion source pressure range from 0.8 to 2.5 Torr. Numbers beside straight lines give temperature in degrees C.

leaving the ion source and collision-induced decomposition, due to collisions with residual gas in the mass spectrometer, one needs to measure the metastables as a function of pressure, by admitting gas in the mass spectrometer tube. Studies of this type, initiated in the potassium hydrate study,[15] were performed also in the present work on the hydronium ions. The information on collision-induced dissociation obtained from these experiments has turned out to be of relevance not only to the measurement of clustering equilibria, but also to the field of collision-induced dissociation[16] (CID) and particularly some recent experiments by Cooks.[17]

(16) McLafferty, F. W.; Bockhoff, F. M. *J. Am. Chem. Soc.* **1979**, *101*, 1783.
(17) McLuckey, S. A.; Cameron, D.; Cooks, R. G. *J. Am. Chem. Soc.* **1981**, *103*, 1313.

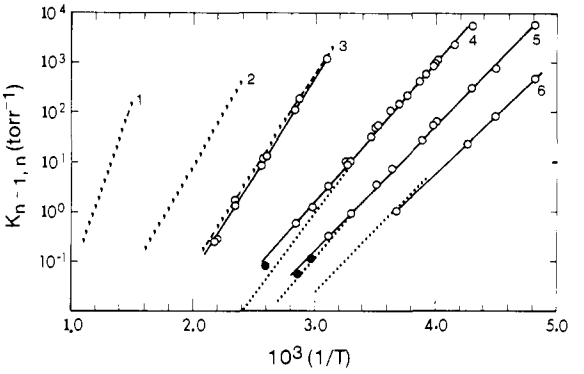

Figure 2. van't Hoff plots of equilibrium constants $K_{n-1,n}$ for reactions $(n-1,,n)$ $H_3O^+(H_2O)_{n-1} + H_2O = H_3O^+(H_2O)_n$: present results (—), Cunningham et al.[11] (---), Searles et al.[10] (•••). All data points are from present work: (○) major gas CH_4, (●) neat H_2O. Plots of Cunningham and Searles are shown over the exact temperature range used in respective experiments. Present data are in good agreement with the Cunningham (2,3) plot. Cunningham (0,1), (1,,2), and (2,3) plots plus present data for $(n-1,n)$ are the "best set" of determinations for the reactions $(n-1,n)$ from this laboratory.

Experimental Section

The measurements were made with a pulsed electron beam high ion source pressure mass spectrometer of design similar to that used in the earlier study.[11] The ion source was positioned inside a massive block. This block could be heated, by means of embedded cartridge heaters, or cooled, by circulating fluid at low temperature through channels milled out in the block. The electron beam entered the ion source axially; i.e., the electron entrance and ion exit slit were mounted coaxially in the axis of the cylindrically symmetrical ion source.

Mass analysis was obtained with a 60°, 15-cm radius magnetic sector. Detection was obtained as usual by counting the pulses from a Chanel-tron ion-electron multiplier.

The gas mixtures CH_4–H_2O were prepared in a thermostated 5-L glass bulb by filling the bulb with CH_4 at near atmospheric pressure and injecting liquid H_2O with a calibrated syringe. This gas mixture was circulated in and out of the ion source at a flow rate considerably higher than the outflow through the ion source exit slits.

I. Equilibrium Constants, Enthalpies, and Entropies of Reactions $H_3O^+(H_2O)_{n-1} + H_2O = H_3O^+(H_2O)_n$

(a) Determination of the Equilibrium Constants at Different Temperatures. An example of the equilibrium determinations is given in Figure 1. Shown are the experimentally determined equilibrium constants $K_{3,4}$ at different constant temperatures. The $K_{n-1,n}$ were evaluated with eq 2, substituting for P_n/P_{n-1} the ob-

$$K_{n-1,n} = P_n/P_{n-1}P_{H_2O} \qquad (2)$$

served equilibrium ion intensities for $H_3O^+(H_2O)_n$ and $H_3O^+(H_2O)_{n-1}$. The concentration conditions in the ion source were such that the two ions generally reached equilibrium within a few hundred microseconds. The results for $K_{3,4}$ given in Figure 1 are typical also for the other determinations. $K_{n-1,n}$ was observed to remain constant for a change of water pressure by a factor of about 3. The selected water partial pressure in the methane major gas was lower in runs at low temperature (see Figure 1). This permitted one to cover a wide temperature while still keeping the $n/(n-1)$ ion ratio not too far from unity. The determinations in Figure 1 cover the temperature range 80 to −40 °C with a variation of $K_{3,4}$ from 0.3 to 6000 (Torr^{-1}). This is as wide a range as is presently possible to obtain without the use of neat water in the ion source.

van't Hoff plots of the data from Figure 1 and similar data for the other equilibria measured in the present work are shown in Figure 2. Included in this figure are also the earlier determinations from this laboratory.[10,11] The present data for $K_{2,3}$ are found in excellent agreement with the more recent determination by Cunningham et al.[11] The equilibria (0,1) and (1,2) previously measured by Cunningham[11] are believed reliable and were not remeasured in the present work. Cunningham et al.[11] determined the equilibria (0,1) – (2,3) with methane as the major gas. They found some deviation of their results from the early measurements

Table I. Data for the Equilibria: $H_3O^+(H_2O)_{n-1} + H_2O = H_3O^+(H_2O)_n$[a]

$(n-1,n)$	$-\Delta H^\circ_{n-1,n}$	$-\Delta S^\circ_{n-1,n}$	$-\Delta G^\circ_{n-1,n}$(300 K)	$-\Delta H^\circ_{n-1,n}$[d]	$-\Delta E_{n-1,n}$[e]
0,1	31.6[b] (36)[c]	24.3[b]	24.3 (25)[c]	33.0	37
1,2	19.5[b] (22)[c]	21.7[b]	13.0 (13.6)[c]	21.0	26
2,3	17.9 (17)[c]	28.4	9.5 (8.5)[c]	16.0	22
3,4	12.7 (15)[c]	23.4	5.6 (5.5)[c]	14.8	16
4,5	11.6 (13)[c]	25.0	4.1 (3.9)[c]		15
5,6	10.7 (12)[c]	26.1	3.0 (2.8)[c]		
6,7	(10)[c]				

[a] ΔH°, ΔG° in kcal mol^{-1}, ΔS° in cal K^{-1} mol^{-1}. Standard state 1 atm. Data in parentheses are previous data from this laboratory which are of lower accuracy than unparenthesized results from this laboratory. [b] Cunningham.[11] [c] Searles.[10] [d] Meot-Ner[12] equilibria measurements. [e] Newton[19] 4-31G calculated energies with zeropoint correction.

by Searles et al.[10] This was ascribed[11,18] to somewhat erroneous temperature readings in the Searles' source at high temperature. Cunningham et al.[11] made a few checks of equilibrium constants $K_{3,4}$ to $K_{5,6}$. These were mostly near-room-temperature determinations. Agreement with the earlier results of Searles et al.[10] was observed.

An examination of Figure 2 shows that the present equilibrium constants for (3,4) to (5,6) agree with those of Searles et al.[10] only near room temperature. The largest part of the plots of Searles et al.,[10] which were obtained with neat water, falls at higher temperatures. The slopes of these plots are seen to be noticeably steeper than those from the present determinations. We believe that the previous determinations were in error. Analysis of some of the factors that might be involved in the deviations is given in section III.

(b) Discussion of the Thermodynamic Results. The present determinations combined with the (0,1) and (1,2) results of Cunningham[11] (see Figure 2) provide a "best set" of $\Delta G^\circ_{n-1,n}$, $\Delta H^\circ_{n-1,n}$, and $\Delta S^\circ_{n-1,n}$ which is given in Table I. Even though the deviations from the data of Searles et al.[10] are not that large, there is a significant qualitative change. This is illustrated in Figure 3 which gives the $\Delta H^\circ_{n-1,n}$ vs. $(n\text{-}1,n)$. The present results show a distinct break after $-\Delta H_{2,3}$; i.e., $-\Delta H^\circ_{3,4}$ is significantly lower than $-\Delta H^\circ_{2,3}$. The data of Searles[10] do not show this brek because $-\Delta H^\circ_{3,4}$ measured in that set was higher. Given in Table I and Figure 3 are also the stabilization energy differences $\Delta E_{n-1,n} = E_n - E_{n-1}$ calculated by Newton[19] with a 4-31G basis set. These values include also the vibrational zero-point energy correction. Newton's results are seen to be slightly higher; however, the trends are exactly the same as in the present results. There are two falloff points in the bonding energies: after the dimer $H_3O^+ \cdot H_2O$ in which the proton is shared, and after $H_3O^+(H_2O)_3$, the Eigen structure which represents the complete inner shell. Figure 3 gives also our previous results[20] for $NH_4^+(NH_3)_n$. Again the pattern of changes is similar, but now the second falloff occurs after $NH_4^+(NH_3)_4$, i.e., the complete inner shell for the ammonium ion.

The best set $\Delta G^\circ_{n-1,n}$ values at 300 K (Table I) are very close to the results of Searles.[10] This is due to differences in the $\Delta S^\circ_{n-1,n}$ values between the two sets, which tend to compensate the $\Delta H^\circ_{n-1,n}$ differences. Plotting $\Delta G^\circ_{n-1,n}$ vs. n, one finds a much less pronounced break after the $H_3O^+(H_2O)_3$ structure; i.e., the noticeable prominence of this structure in the ΔH° plots has almost disappeared in the ΔG° plots (see Figure 3).

The set of best $\Delta H^\circ_{n-1,n}$ and $\Delta S^\circ_{n-1,n}$ values in Table 2 permits one to calculate the free-energy change at different temperatures T with the equation $\Delta G^\circ = \Delta H^\circ - T\Delta S^\circ$. This in turn can be used to evaluate $K_{n-1,n}$ (atm^{-1}) via the equation $-RT \ln K = \Delta G^\circ$. The equilibrium constants in their turn can be used to evaluate the relative concentrations of the hydrates $H_3O^+(H_2O)_n$ for a wide variety of H_2O gas presures and temperatures. Examples of such calculated distributions were given in Figure 6 of our previous publication (Searles[10]).

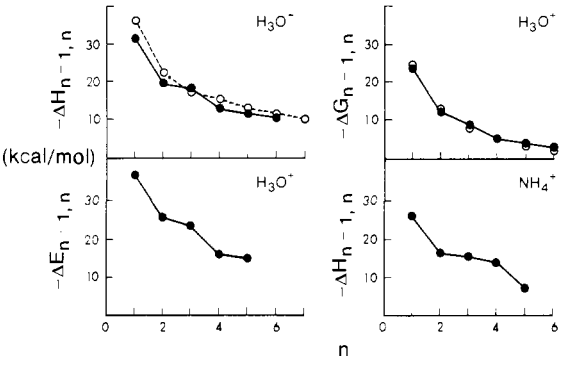

Figure 3. Energy changes for reactions $(n-1,n)$. Top figure: $\Delta H^0_{n-1,n}$ for reaction $H_3O^+(H_2O)_{n-1} + H_2O = H_3O^+(H_2O)_n$. (●) Present results from Table I; (○) earlier data from this laboratory (Searles[10]). Present data show stability decrease after $H_3O^+(H_2O)_3$, which was not evident from Searles[10] data. $\Delta E_{n-1,n}$ are 4-31G calculated energy changes of Newton.[19] Present data and Newton's calculations show the same pattern of changes. The bottom figure gives $\Delta H^0_{n-1,n}$ for the reaction $NH_4^+(NH_3)_{n-1} + NH_3 = NH_4^+(NH_3)_n$ (Payzant[20]) which shows a similar pattern, of interactions; however, falloff occurs after $NH_4^+(NH_3)_4$, as expected.

II. Kinetics of the H_3O^+ Hydration

(a) Determination of the Rate Constants at Different Temperatures. The hydration reactions (eq 1) are exothermic association reactions which at low pressures are expected to be third order in the forward direction and second order in the reverse direction. At high pressures the forward reaction becomes second order and the reverse reaction first order.

Reactions 1 represent a system of consecutive reversible reactions. One way to obtain rate constants is to fit the time dependence of normalized ion intensities with a computer. Fits with an analog computer were used in some of our previous work.[21] In the present determinations a numerical technique was applied which is somewhat simpler and has the advantage that the fit does not depend on the values of the equilibrium constants for the reversible reactions, as is the case with the computer fit. The present approach is illustrated in Figures 4 and 5. Figure 4a gives the normalized ion intensities of one run used for the determination of the rate constant k_3. The numbering of the rate constants is defined in eq 3. We call the reacting ion A (A = $H_3O^+(H_2O)_2$

$$H_3O^+(H_2O)_{n-1} + H_2O + CH_4 \xrightarrow{k_n} H_3O^+(H_2O)_n + CH_4 \quad (3)$$

in the present case) and the product ions B and C (B = $H_3O^+(H_2O)_3$; C = $H_3O^+(H_2O)_4$). In the early stages of the reaction where B and C are small, the reverse rate is also small. For this condition the reaction frequency ν_n defined in (4) is given

$$\text{reaction frequency} = \nu = k[H_2O][CH_4] \quad (4)$$

by (5). The integral representing the area under A is evaluated

$$(B_t - B_{t_0}) + (C_t - C_{t_0}) = \nu_n \int_{t_0}^{t} A\, dt \quad (5)$$

(18) Payzant, J. D. Ph.D. Thesis, "Kinetics and Equilibrla of Ion Molecule Reactions", University of Alberta, Edmonton, 1973.

(19) Newton, M. D. *J. Chem. Phys.* **1977**, *67*, 5535. For other theoretical results see: Diercksen, G. H. F.; Kraemer, W. P.; Roos, B. O. *Theor. Chim. Acta* **1975**, *36*, 249. Kraemer, W. P.; Diercksen, G. H. F. *Chem. Phys. Lett.* **1970**, *5*, 463.

(20) Payzant, J. D.; Cunningham, A. J.; Kebarle, P. *Can. J. Chem.* **1973**, *51*, 3242.

(21) French, A. M.; Hills, L. P.; Kebarle, P. *Can. J. Chem.* **1973**, *51*, 1973.

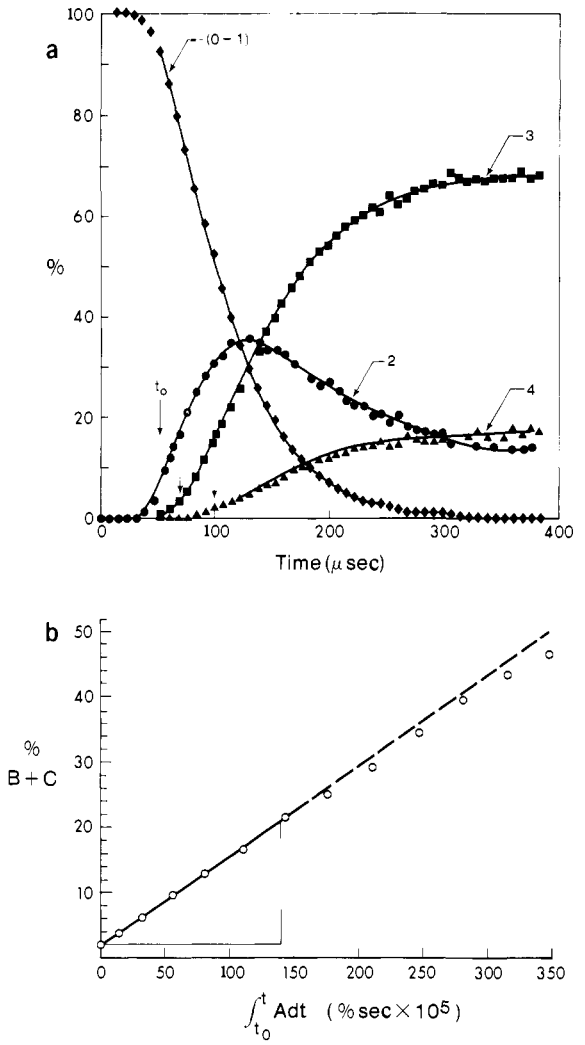

Figure 4. (a) Time dependence of normalized ion intensities (=ion intensities expressed as % of total ionization) in a run used for the determination of the rate constant k_3 for the reaction $H_3O^+(H_2O)_2 + H_2O + CH_4 = H_3O^+(H_2O)_3 + CH_4$. Numbers beside curves give values of n in $H_3O^+(H_2O)_n$. t_0 corresponds to start of plot shown in Figure 4b. The time between successive experimental points is 10 μs. Reactions approach equilibrium above 300 μs: temperature −40 °C; $p(CH_4) = 1.17$ Torr; $p(H_2O) = 0.83 \times 10^{-3}$ Torr. (b) Determination of rate constant k_3 for reaction $H_3O^+(H_2O)_2 + H_2O + CH_4 = H_3O^+(H_2O)_3 + CH_4$ from data shown in Figure 4a. A = $H_3O^+(H_2O)_2$; B = $H_3O^+(H_2O)_3$; C = $H_3O^+(H_2O)_4$. According to eq 5, the plot leads to an initial slope which is equal to reaction frequency $\nu_3 = k_3[H_2O][CH_4]$. Falloff in slope is due to increased contribution of the reverse reaction at long reaction times; time between successive points equals 10 μs; total extent of plot in figure is ~120 μs. The equilibrium is near complete at $t > 300$ μs (see Figure 4a).

numerically from the concentrations of A, while B and C are obtained directly from the normalized intensities (see Figure 4a). A plot corresponding to eq 5 is shown in Figure 4b. It will be noted that the plot is almost linear, but that an (expected) gradual decrease of slope occurs for longer times where the reverse rate of the reaction becomes noticeable. The initial slope, which should not be affected by the reverse reaction, was taken as equal to ν_n (ν_3 in the present case); k_n can then be evaluated from the known water and methane concentrations and eq 4.

All the rate constant determinations were made in runs which were quite separate from the runs used for the equilibrium measurements (see section I). The water pressures were kept in the region of 1 to a few mTorr while the methane pressure was ~1 Torr. In general, conditions were sought which lead to A going to zero at long reaction times so as not to have a reversible component. Such conditions could not be always obtained. However, in most cases the results were based on a fairly long linear portion in the plot of eq 5 as shown in Figure 4b.

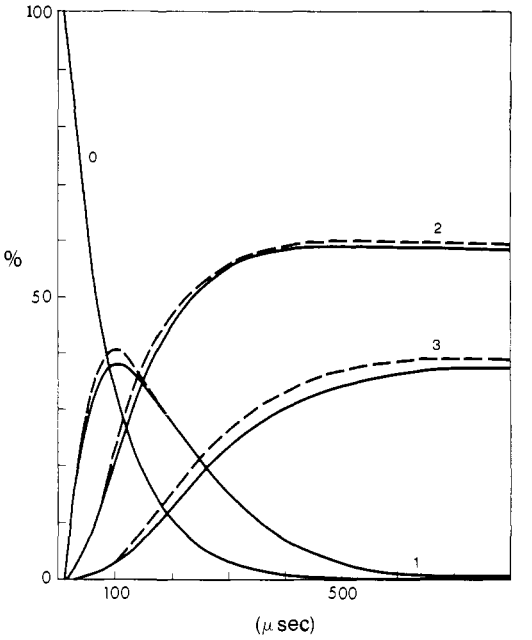

Figure 5. Analog computer fit of rate constants k_n for reactions $H_3O^+(H_2O)_{n-1} + H_2O + CH_4 = H_3O^+(H_2O)_n + CH_4$: (—) analog computer fit, (---) experimental. Computer fit leads to rate constants $k_1 = 2.9 \times 10^{-27}$, $k_2 = 2.6 \times 10^{-27}$, $k_3 = 1.1 \times 10^{-27}$, $k_{-2} = 1.2 \times 10^{-15}$, $k_{-3} = 2.8 \times 10^{-13}$. Rate constants obtained from plots like those in Figure 4 (summarized in Figure 6) are $k_1 = 2.2 \times 10^{-27}$, $k_2 = 2.8 \times 10^{-27}$, $k_3 = 1.1 \times 10^{-27}$. Reverse rate constants are calculated from above and equilibrium constants from Figure 2: $k_{-2} = 1.7 \times 10^{-15}$; $k_{-3} = 2.8 \times 10^{-13}$. All forward rate constants are in cm^6 $molecule^{-2}$ s^{-1}; reverse in cm^3 $molecule^{-1}$ s^{-1}; temp 79 °C, $p(H_2O) = 5.9$ mTorr, $p(CH_4) = 0.8$ Torr. Numbers beside curves correspond to n in $H_3O^+(H_2O)_n$.

Checks were made to establish that a measured ν_n at a given temperature is proportional to the H_2O concentration; however, the total concentration of the third body was not changed over a wide range since this would have meant much more extensive measurements. The third body dependence of the (forward) rate constant is more easily established via the log k_n vs. log T plots shown in Figure 6. These are discussed in the next section.

Some checks were made with the analog computer in order to examine the quality of the fit obtained with the rate constants from Figure 6 and the equilibrium constants from Figure 2. An example is given in Figure 5, which shows such an analog computer fit. The rate constants from that fit are seen to be in good agreement with the rate constants of the plots in Figure 6 and the equilibrium constants from the independent equilibrium determinations (Figure 2 and Table I).

(b) Summary and Discussion of Rate Constant Data. The rate constants k_n for the hydration reactions defined in eq 3 are shown in Figure 6 as log k_n vs. log T plots. As was mentioned in the preceding section, the reaction frequencies (pseudo-first-order rate constants), $\nu_n = k_n[H_2O][CH_4]$, were mostly measured at constant concentration of methane; i.e., we did not establish, by measuring the pressure dependence of the third body, whether the reaction is third order or second order. The rate constants k_n shown in Figure 6 were calculated from the corresponding ν_n under the assumption that the reactions are third order. By examining the temperature dependence of the rate constants it is easy to establish whether the rate was really third order. Third-order rate constants have a strong negative temperature dependence which can be expressed by the empirical equation

$$k = aT^{-b} \tag{6}$$

This relationship leads to linear log k vs. log T plots.[12,22] On the other hand, the second-order rate constants involving dipolar molecules like H_2O have only an extremely weak negative temperature dependence (see ADO theory[23]). Therefore, the linear

(22) Hiraoka, K.; Kebarle, P. *J. Chem. Phys.* **1975**, *63*, 746.

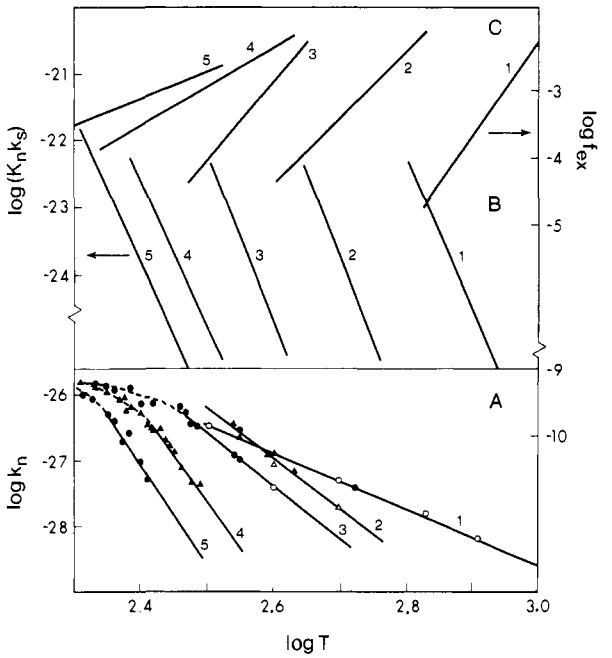

Figure 6. (A) Logarithmic plot of $\nu_n/[H_2O][CH_4]$ vs. temperature. ν_n is the reaction frequency (pseudo-first-order rate constant) for the reactions $H_3O^+(H_2O)_{n-1} + H_2O + CH_4 = H_3O^+(H_2O)_n + CH_4$. The concentration of methane was kept approximately constant at $[CH_4] \approx 4 \times 10^{16}$ molecules/cm^3. Linear portion of plots corresponds to region where reactions are third order and obey relationship 6: $k_n = aT^{-b}$, where $k_n = \nu_n/[H_2O][CH_4]$. The region of curvature occurring at low temperatures correspond to the regime where the reaction is intermediate between second and third order. Near zero slope is expected for the pure second-order region. The scale of the ordinate on the left is calculated for third-order rate constants, on right for second-order; i.e., the scale of the ordinate on the right corresponds to $\nu_n/[H_2O]$: shaded symbols, present work; unshaded symbols, earlier work from this laboratory.[11] (B) Plot of log $(k_s K_n)$ vs. log T. K_n are equilibrium constants for reactions $H_3O^+(H_2O)_{n-1} + CH_4 = H_3O^+(H_2O)_n + CH_4$ expressed in units (molecules/cm^3)$^{-1}$. These were obtained from $K_{n-1,n}$ (Torr^{-1}). k_s is stabilization rate constant; see eq 7 and 16. $k_s = k$(Langevin) is constant with temperature. (C) Plot of log $f_{ex}^{(n)}$ vs. log T. $f_{ex}^{(n)}$ corresponds to fraction of clusters n excited above dissociation limit $\Delta H^0_{n,n-1}$. $f_{ex}^{(n)}$ was evaluted from eq 16 and experimentally determined K_n and k_n.

portions in the plots of Figure 6 must be corresponding to temperatures where the rate constants are third order. The low-temperature portion of the plots where there is a decrease of slope resulting in noticeable curvature will be the region where the order is intermediate between third and second order. Finally a region of near-zero slope is expected where the reaction is second order. In that region, $\nu_n = k_n^{(2)}[H_2O]$ and the second order $k_n^{(2)}$ will be close to 10^{-9} cm^3 molecule^{-1} s^{-1}. The line corresponding to 10^{-9} is shown in Figure 6. The curves are seen to be approaching this line in their low-temperature region of very small slope. Thus, in this region, the reactions are very near to second order (at $\sim$1 Torr CH_4).

The plots for the rate constants k_2 include two additional points and that for k_3 includes one additional point obtained in previous determinations from this laboratory (Cunningham[11]). These points are found in very good agreement with the present work. Therefore, we did not do a completely new determination of k_1 whose temperature dependence was studied by Cunningham.[11]

The parameters a and b of eq 6 corresponding to the straight-line relationship for k_n in Figure 6 are given in Table II.

Information on k_1 from the literature and the present results is summarized in Figure 7. The earlier results of Cunningham[11] and the present experimental points are seen to be in fairly good agreement. These are in fair agreement with Meot-Ner and Field's[12] data, particularly near room temperature. The present line and Field's data predict the same k_1 at 300 K. This result

(23) Su, T.; Bowers, M. T. *J. Chem. Phys.* **1973**, *58*, 3027.

Table II. Temperature Dependence of Third-Order Rate Constants k_n for Reactions $(H_2O)_{n-1} + H_2O + CH_4 = H_3O^+(H_2O)_n + CH_4$[a]

n	a	b	a^*	b^*
1	3.7×10^{-17}	4	2×10^{-30}	0
2	$4.1 \times 10^{-8.1}$	7.5	5×10^{-19}	3.9
3	4.2×10^{-7}	8.1	2×10^{-9}	7.2
4	2.2×10^{7}	14	3×10^{-1}	10.4
5	4.6×10^{9}	15.3	4×10^{6}	13.3

[a] Values of parameters a and b of the equation $k = aT^{-b}$. Values of a and b give rate constants in molecules^{-2} cm^6 s^{-1}. Values of a and b were obtained from straight-line portions of plots in Figure 6. Values of a^* and b^* refer to rate constant k_n for hydrations of the potassium ion $K^+(H_2O)_{n-1} + H_2O + M = K^+(H_2O)_n + M$. These are calculated results obtained from eq 16 and $K_{n-1,n}$ and f_{ex} obtained by Sunner et al.[15]

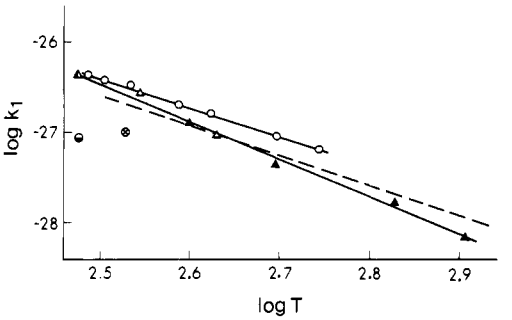

Figure 7. Data for the reaction $H_3O^+ + H_2O + CH_4 = H_3O^+(H_2O) + CH_4$: (△) present work, (▲) Cunningham et al.[11], (○) Meot-Ner and Field,[12] (△) Good et al.[13] (M = N_2 converted to M = CH_4), (⊗) Young et al.[24] (M = Ar converted to M = CH_4), (◒) theoretical result by Golden.[27] (---) Theoretical prediction was obtained with eq 16, $K_{0,1}$ (Cunningham et al.[11]); f_{ex} calculated from normal frequencies of $H_3O^+H_2O$.

is in complete agreement with an earlier determination from this laboratory by Good et al.[13] made with N_2 as third body. The value used in Figure 7 has been corrected to CH_4 for third body by multiplying by the Langevin rate constant ratio $k_L(CH_4)/k_L(N_2) = 1.13/0.78$. This assumes that the stabilization rate constants by the third body are proportional to the corresponding orbiting collision rate constants. The determination by Young et al.[24] obtained at 337 K with Ar as third body was multiplied by a factor 1.13/0.67 in order to convert it to methane as third body. This result is lower by a factor of about 4 from the present and Field's results. Young's[24] determination depended on an extrapolation (see Figure 9, ref 24) in which there was a very large scatter of the experimental points. This indicates that Young's result probably is unreliable.

The linear sections of the plots of the rate constants k_n in Figure 6 follow a regular pattern. The (negative) slope of the lines increases with n. A second change is a gradual shift of the lines toward lower temperatures, with increasing n. Thus a given fixed value of k_n (say, 10^{-27} cm^6 molecule^{-2} s^{-1}) is reached at lower and lower temperatures for increasing n. Since some of the plots cross, a simple dependence of k_n on n at a given constant temperature T cannot be generally expected. For example, at T = 300 K, $k_1 \approx 5$, $k_2 \approx 9$, $k_3 \approx 4$, $k_4 \approx 0.5$, $k_5 \approx 0.05$ (all in 10^{27} cm^6 molecule^{-2} s^{-1}; see Table II).

It is interesting to note that the pattern of the log k_n lines is similar to the pattern of stabilities of the hydrates observed in the thermodynamic mesurements (Figure 2). Thus log k_1 is a line apart from the others (like log $K_{0,1}$). Then log k_2 and log k_3 are closer together and of similar slope as were log $K_{1,2}$ and log $K_{2,3}$ in Figure 2; then there is a larger gap followed by closely spaced and of similar slope log k_4 and log k_5 (respectively log $K_{3,4}$ and log $K_{4,5}$).

Association reactions like (1) are generally represented by the strong collision mechanism

(24) Young, C. E.; Edelson, D.; Falconer, W. E. *J. Chem. Phys.* **1979**, *53*, 4296.

$$A + B \underset{k_d}{\overset{k_c}{\rightleftharpoons}} AB^* \underset{k_a[M]}{\overset{k_s[M]}{\rightleftharpoons}} AB \tag{7}$$

$$A + B \underset{k_r}{\overset{k_f}{\rightleftharpoons}} AB \tag{8}$$

involving the third body M. A simplified qualitative approach proceeds as follows. A steady-state treatment of (7) leads to (9).

$$k_f = \frac{k_c k_s[M]}{k_d + k_s[M]} \qquad k_r = \frac{k_a k_d[M]}{k_d + k_s[M]} \tag{9}$$

At low pressures where condition 10 holds, these relationships

$$k_s[M] << k_d \tag{10}$$

simplify to the relationships shown in (11) where $k^{(3)}$ and $k^{(2)}$ stand

$$\begin{aligned} k_f^0 &= k_c k_s[M]/k_d \qquad & k_r^0 &= k_a[M] \\ k^{(3)} &= k_c k_s/k_d \qquad & k^{(2)} &= k_a \end{aligned} \tag{11}$$

for the third-order rate constant in the forward and $k^{(2)}$ the second-order rate constant in the reverse direction. Generally, both k_c and k_s are assumed to be approximately given by the corresponding ADO orbiting collision expressions. This means the product $k_c k_s$ is expected to be near 10^{-18} (cm^6 $molecule^{-2}$ s^{-1}) and largely temperature independent. The simplified Kassel equation

$$k_d \approx A\left(\frac{\nu RT}{E_0 + \nu RT}\right)^{s-1} \tag{12}$$

$$\nu \approx 2s;\ E^0 \approx \Delta H^0_{n,n-1}$$

has been used at times[25] to obtain qualitative predictions for k_d. s is the number of active vibrations and ν is the number of equipartitioned internal degrees of freedom in the complex AB. E^0 is the critical energy, i.e., the minumum energy required for the dissociation of AB. Substituting (12) into (11) for $k^{(3)}$ one obtains (13). Equation 14 results from the assumption that

$$k^{(3)} \approx \frac{10^{-18}}{A}\left(\frac{\Delta H^0 n,n-1 + \nu RT}{\nu RT}\right)^{s-1} \tag{13}$$

$$k^{(3)} \approx \frac{10^{-18}}{A}\left(\frac{\Delta H^0_{n,n-1}}{\nu R}\right)^{s-1} T^{-(s-1)} \tag{14}$$

$\Delta H^0_{n,n-1} >> \nu RT$ which is true at moderate and low temperatures. Equation 14 is of the same form as the empirical eq 6, $k = aT^{-b}$. The change of a with n should be reflected in the change of $(\Delta H^0_{n,n-1}/\nu R)^{s-1}$. Since $\Delta H^0_{n,n-1}$ decreases slowly with n, while ν and s increase in proportion with n, eq 14 predicts an increase of a with n. An increase is observed in the experimental values of a given in Table II. According to (14), $(s-1) \approx b$, and since s increases with n, b should increase likewise. Again an increase is observed in the experimental values for b. Thus, 13 and 14 do provide a crude explanation of the observed trends. However, if one needs anything more quantitative, one must take recourse to more detailed treatments.

In a more exact treatment,[26] one applies the steady-state assumption not to (7) but to a microcanonical ensemble dealing with $AB^*(E)$, and the corresponding $k_d(E)$, $k_a(E)$, and $k_c(E)$. A dependence of k_s on the internal energy of AB^* is normally not taken into account. Integration over all values of E of $AB^*(E)$ (i.e., from E_0 to ∞) leads[26] to a particularly simple result for the rate constant of the reverse reaction in the low-pressure region. This result is given in the equation

$$k^{(2)} = k_s f_{ex} \tag{15}$$

where

$$f_{ex} = \frac{[AB^*]}{[AB]} = \frac{Q_{AB^*}}{Q_{AB}}$$

$[AB^*]$ is the concentration of all AB molecules excited above the critical energy E_0 at thermal equilibrium. Q_{AB^*} and Q_{AB} are the corresponding partition functions. f_{ex} can be evaluated (at least approximately) by standard methods provided that the frequencies of the normal vibrations of AB are known and E_0 is available. For k_s one can take the corresponding ADO rate constant. Using the equilibrium expression, one obtains (16) for the third-order

$$K = k^{(3)}/k^{(2)} \qquad k^{(3)} = K k_s f_{ex} \tag{16}$$

rate constant of the forward reaction. Thus, one can calculate $k^{(3)}$ if K and f_{ex} are available, or conversely one can evaluate f_{ex} if K and $k^{(3)}$ are available. The latter approach was taken in the recent publication from this laboratory[15] which concerned itself with the possible decomposition of ions AB^* in the mass analysis tube of the apparatus used to measure ion equilibria. More recently, Chang and Golden[27] evaluated a number of rate constants $k^{(3)}$ with eq 16 from experimentally measured equilibrium constants K and from f_{ex} based on estimated vibrational frequencies.

The f_{ex} evaluated for $H_3O^+ \cdot H_2O$ in Sunner's[15] work for different temperatures, together with $K_{0,1}$ from Table I and k_s (the Langevin rate constant for collisions of CH_4 and $H_3O^+ \cdot H_2O$), were used to obtain the theoretical prediction of the temperature dependence of k_1 in the third-order region shown in Figure 7. The theoretical line fits the experimental plot quite closely. A few years ago, Braumann et al.[28] calculated k_1 in the third order and the intermediate pressure region. An RRKM calculation and assumptions about the nature of the transition complex of AB^* are required for the intermediate region. The Brauman results for the third-order region should be essentially identical with the present evaluation of k_1 since the basic data input is the same in both calculations. Chang and Golden[27] have also made a calculation of k_1 but only at room temperature. They also used the same basic data, but evaluated f_{ex} by a different method.[29] Their value for k_1, shown in Figure 7, is not in very close agreement with the present experimental results.

It might be possible to estimate fairly reliable f_{ex} for the higher H_3O^+ hydrates. These will lead, via (16), to the temperature dependence of the rate constants k_n. The required frequencies of the normal vibrations of the hydrates could be estimated by an approach similar to that used for $H_3O^+ \cdot H_2O$. In that case[28] frequencies were selected which led to a calculated $\Delta S^0_{0,1}$ which agreed with the experimental[11] determination. The evaluation of ΔS involves also the rotational changes so that one needs to know the moments of inertia. These could be obtained from the theoretical results of Newton[19] which give the most stable geometries for $H_3O^+(H_2O)_n$. Additional guidance would be provided by the experimental vibrational spectra of $H_3O^+(H_2O)_3$ of Schwarz.[30] We have not yet made such calculations. The already existing theoretical f_{ex} for the potassium ion hydrates $K^+(H_2O)_n$ (Sunner[15]), together with available equilibrium constants for the same system, permit the evaluation of $k_n^{(3)}$ for this system. These results provide an interesting comparison with the data for the hydronium ion. The theoretically predicted rate constants are given in Table II. The results for potassium show some similarity to those for the hydronium ion. The exponents b increase with n; however, these increases are much more regular. Also the factors a increase more regularly. The potassium hydrate frequencies were calculated[15] for the most symmetric structures in which all H_2O molecules were equivalent (n = 1 to 4) or near equivalent (n = 5 trigonal bipyramid). Thus the observed regularity is not surprising, as there are no drastic changes of structure as in the case of $H_3O^+(H_2O)_n$. One can understand easily some of the other qualitative differences. Thus the $b \approx 4$ (H_3O^+) vs. $b \approx 0$ (K^+) for the exponents in k_1 undoubtedly reflects the large

(25) Good, A. *Chem. Rev.* **1975**, *75*, 561.
(26) Robinson, P. J.; Holbrook, K. A. "Unimolecular Reactions"; Wiley-Interscience: London, 1972.
(27) Chang, J. S.; Golden, D. M. *J. Am. Chem. Soc.* **1981**, *103*, 496.
(28) Jasinski, J. M.; Rosenfeld, R. N.; Golden, D. M.; Braumann, J. I. *J. Am. Chem. Soc.* **1979**, *101*, 2259.
(29) Troe, J. *J. Chem. Phys.* **1977**, *66*, 4758.
(30) Schwarz, H. A. *J. Chem. Phys.* **1977**, *67*, 5525.

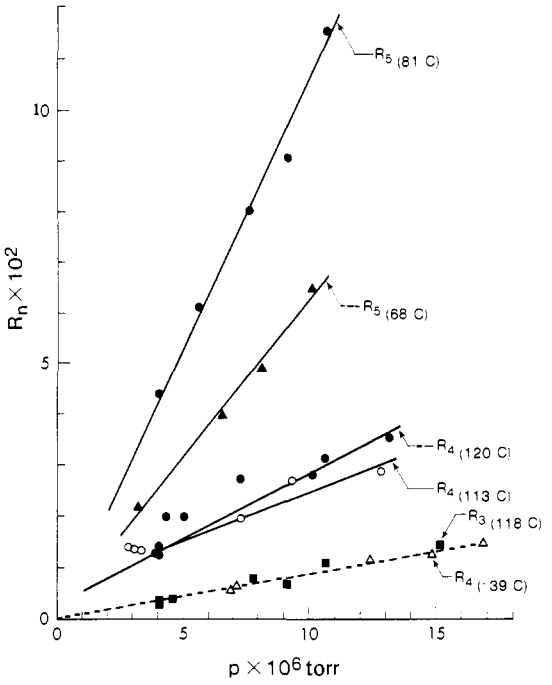

Figure 8. Plot of R_n vs. pressure in mass analysis tube. R_n is the ratio of "metastable" ions $H_3O^+(H_2O)_n \rightarrow H_2O^+(H_2O)_{n-1}$ over ions detected as $H_3O^+(H_2O)_n$. Temperatures given correspond to those of ion source. Linearity of R_n with pressure indicates that all metastables are due to (single) collision-induced dissociation (CID) with target gas. Results show that CID cross sections increase rapidly with n. This probably is due to decrease of dissociation energy ($\Delta H^0_{n,n-1}$) with n. The CID cross sections are also dependent on the temperature of the ion source, i.e., on the internal energy of the clusters n. Clusters with large n (i.e., R_5) show the largest temperature dependence. These have the highest heat capacity and lowest dissociation energy. Pressure given in abscissa represents actual ion gauge reading. It must be multiplied by ~1.6 to obtain expected ion gauge reading at mass analysis tube. Ion gauge readings were not corrected for different sensitivity to air, CH_4, and H_2O: (Δ) R_4 (−39 °C); (○) R_4 (113 °C); (■) R_3 (118 °C).

difference of internal degrees of freedom between $H_3O^+(H_2O)$ and $K^+(H_2O)$.

It would be very interesting to compare the predicted rate constants k_n for potassium with actually measured values. Unfortunately kinetic measurements with our thermionic ion source[31] of K^+ are not directly feasible. We have recently started kinetic measurements for the hydrates of Cl^-, expecting that they will show a behavior similar to that of K^+.

Equation 16 and the known equilibrium constants $K_{n-1,n}$ for the hydronium ions (Table I) were used for the evaluation of f_{ex} of the hydronium hydrates. These together with the corresponding equilibrium constants are plotted as log f_{ex} (respectively log $K_{n-1,n}$) vs. log T in Figure 6. Straight lines are obtained over the temperature range covered. The composite plots A, B, and C in Figure 6 provide an illustration of the effects of the equilibrium constants and f_{ex} on the respective rate constants k_n.

III. Unimolecular and Collisional Dissociation in the Mass Analysis System

(a) Dependence of CID on Internal Energy of Ions. An earlier study from this laboratory[15] demonstrated that easily detectable CID of clusters $K^+(H_2O)_n$ occurs in the mass analysis system owing to collisions with "background" gas at pressures as low as 10^{-6} Torr. It was also established that the CID cross sections increased rapidly with the number (n) of water molecules in the cluster. Similar experiments were made in the present study; however, this time also the dependence of the CID cross sections on the internal energy of the clusters was examined. The results are presented in Figure 8. R_n, the metastable ratio for cluster n, is defined in (17). The approximate straight lines obtained

$$R_n = \frac{\text{clusters } n \text{ dissociating to } n-1 \text{ in metastable region}}{\text{clusters detected as } n} \quad (17)$$

in the plots R_n vs. ion tube pressure and the small values of R_n indicate that thin target conditions obtain; i.e., only single collisions are involved. Therefore, the slopes of the lines are proportional to the CID collision cross sections. It is observed that the cross sections (at constant ion source temperature) increase in the order R_3, R_4, R_5, an observation made already in the earlier study.[15] New is the finding that the cross sections increase also with the temperature of the ion source. Since the clusters leaving the ion source have near thermal energy distributions, this means that the CID cross sections increase rapidly with the internal energy of the ions. The effect of temperature is found to be much larger for R_5 than R_4. This probably is connected with the higher heat capacity and the lower dissociation energy ($\Delta H^0_{n,n-1}$) of the larger cluster. The data show that at a constant temperature (120 °C) the CID cross section for $n = 4$ is more than twice as large as that for $n = 3$. An even larger ratio could be deduced for $n = 5$ and $n = 4$ from Figure 8. Since the geometric cross section of the two clusters could not differ by such a large factor, this observation also indicates that the CID cross section increases with decrease of the dissociation energy $\Delta H^0_{n,n-1}$. It is evident that the small scattering angle collisions producing the observed metastable dissociation induce rather small excitation energies in the clusters. Otherwise, the strong dependence on temperature and $\Delta H^0_{n,n-1}$ would not have been observed. The excitation energies (per collision) probably are in the neighborhood of the $\Delta H^0_{n,n-1}$ involved. This puts them in the 10-kcal/mol range. Approximate CID cross sections can be evaluated from the data in Figure 8. The length of the metastable region is $L = 26$ cm (15-cm radius, 60° sector, single-focusing mass spectrometer). Assuming that this length equals the length of the collision cell, one can calculate the cross section from the thin target equation: $R_n = \sigma_n N/L$, where N is the number of gas molecules per unit volume in the tube and σ_n is the CID cross section. For example, a value of $\sigma_4 = 22 \times 10^{-16}$ cm^2 is obtained from R_4 at 120 °C.

McLafferty and Bockhoff[16] when interpreting CID spectra make the assumption that these spectra are independent of the internal energy residing in the ion prior to the collision.[16] There are a number of differences between the experimental conditions of McLafferty and the present experiments which make a comparison difficult. However, the present results do establish that collisions with very sizable cross sections deposit rather small energies into the ions. When the collision provides only a small excitation energy, a dependence of the fragmentation pattern of the ion on the initial internal energy of the ion must be expected.

Cooks et al.[17] have recently described a method for determining proton affinities by observing the dissociation of proton-bound dimers BH^+B_0 with a mass spectrometer. The proton-bound dimers are produced in a chemical ionization source. The decomposition of BHB_0^+, according to Cooks, is either spontaneous, i.e., the proton bound dimer is metastable and decomposes in the vacuum of the mass spectrometer, or can be induced by introducing a collision gas in a collision cell.

It is somewhat difficult to understand why proton-bound dimers emerging from a chemical ionization source should decompose in the vacuum region. Assuming that the BHB_0^+ are near thermal when they emerge from the ion source, one would expect that the fraction excited above the dissociation limit (f_{ex}) is very small indeed at the 425 K temperature of Cooks[17] ion source. The equilibria $BHB_0^+ \rightleftarrows BH^+ + B_0$ are measured[32] at much higher temperatures and even at those temperatures f_{ex} is expected to be very small because BHB_0^+ do not have many loose normal vibrations and are quite strongly bonded (dissociation energies over 20 kcal/mol).

The results in Figure 8 show that CID decompositions can be observed at mass analysis tube pressures in the 10^{-6} Torr region. Therefore, it is possible that the dissociations observed by Cooks

(31) Davidson, W. R.; Kebarle, P. *J. Am. Chem. Soc.* **1976**, *98*, 6125.

(32) Yamdagni, R.; Kebarle, P. *J. Am. Chem. Soc.* **1973**, *95*, 3504.

in the absence of a collision gas are not spontaneous (true metastables) but are also CID, caused by residual gas pressure in the 10^{-6} Torr range in the ion path. This residual pressure is due to the rather high pressure (0.2-0.5 Torr) used in the chemical ionization ion source.

(b) Unimolecular and CID Decomposition of Ion Clusters and Cluster Equilibria Measurements. It was mentioned in the Introduction that when ion clustering equilibria are measured using the neat clustering gas in the ion source, the desirable condition $f_{ex} << 1$ may not be present at the high-temperature end of the van't Hoff plots. In part II we described how $f_{ex}^{(n)}$ for $H_3O^+(H_2O)_n$ can be determined from eq 16. The high-temperature end for the present measurements was extended up to the point where the equilibrium constants had decreased to the value 0.1 $Torr^{-1}$, for $n = 3$, 4, and 5 (see Figure 2). The $f_{ex}^{(n)}(H_3O^+)$ at the corresponding temperatures are 0.015, 0.004, and 0.002, respectively. The earlier[15] evaluated $f_{ex}^{(n)}(K^+)$ for the same n and same condition ($K_{n-1,n} = 0.1$ $Torr^{-1}$) are 0.09, 0.3, and 0.6, respectively. Both sets of values must be considered only as approximate. Yet the differences between the two systems are sufficiently large to allow the conclusion that the conditions for the present measurements of $H_3O^+(H_2O)_n$ are safe, while this is not the case for the potassium system for $n > 4$.

In the earlier H_3O^+ work (Searles[10]) the measurements extended to $K_{n-1,n}$ as low as 0.01 $Torr^{-1}$. However, most of the experimental points were obtained for equilibrium constants higher than 0.1 $Torr^{-1}$ (see Figure 2). Therefore, the steeper slopes in the Searles' measurements also cannot be caused by too high values of f_{ex}.

The results in Figure 8 indicate that the $H_3O^+(H_2O)_5/H_3O^+(H_2O)_4$ ratio, if measured at ion-tube pressures in the 10^{-5} - 10^{-4} Torr range, will be strongly affected by CID. Not only will the detected ion intensity for $n = 5$ be significantly lowered by CID, but this lowering will increase with temperature. The net result will be an increase of the negative slope of the van't Hoff plot for the (4,5) equilibrium and $-\Delta H^0_{n-1,n}$ and $-\Delta S^0_{n-1,n}$ values which are too high. Of course, this instrumental artifact will also manifest itself in a lowering of the observed equilibrium constant $K_{n-1,n}$ with pressure (at constant temperature) in the vacuum system. Such an effect was observed in the present apparatus. Unfortunately, the mass analysis pressure in the Searles'[10] experiments was not recorded. We do not know whether in that vacuum system the residual pressure was high enough to cause significant CID error. The equilibrium constants in that work were found to be largely independent of ion source pressure. This would not have been the case had CID due to residual gas pressure been involved. Therefore we are not able to pinpoint the cause which affected the Searles'[10] measurements. Nevertheless, the present CID results in Figure 8 are of importance to ion-association equilibria measurements. They show that serious CID can occur if the vacuum system is above 10^{-5} Torr. Furthermore, because of the dependence of CID on the temperature of the ion source, the ion transmission does not only decrease with n but also with temperature.

Registry No. H_3O^+, 13968-08-6; $H_3O^+(H_2O)$, 22206-74-2; $H_3O^+(H_2O)_2$, 23108-28-3; $H_3O^+(H_2O)_3$, 12501-73-4; $H_3O^+(H_2O)_4$, 26719-17-5; $H_3O^+(H_2O)_5$, 40192-94-7; $H_3O^+(H_2O)_6$, 15690-19-4.

Energy Storage and Reaction Pathways in the First Step of the Vision Process

Arieh Warshel* and Natalia Barboy

Contribution from the Department of Chemistry, University of Southern California, University Park, Los Angeles, California 90007. *Received May 26, 1981*

Abstract: The energy storage, resonance Raman spectra, molecular structure, and pathways of formation of the first intermediate in the vision process (bathorhodopsin) are analyzed. The analysis involves a simulation of the protein constraint by an effective steric potential, assuming a limited relaxation of the protein cavity during the isomerization time. It is found that a reasonable estimate of the protein flexibility confines the isomerization pathway in a unique way and simulates the trapping of bathorhodopsin as a strained type intermediate. Adjusting the single parameter that represents the protein rigidity to simulate the energy storage and resonance Raman lines of bathorhodopsin leads to a quite unique prediction of its structure and explains the difference in quantum yield for the formation of bathorhodopsin from rhodopsin and isorhodopsin.

The first step of the vision process involves absorption of light by rhodopsin molecules and a very fast and efficient conversion to the intermediate bathorhodopsin (also known as prelumirhodopsin) (for a recent review, see ref 1). The chromophore of rhodopsin is a protonated Schiff base of retinal (PSBR) in the 11-cis conformation. The conformation of this chromophore in bathorhodopsin is not known, and its characterization is essential for detailed understanding of the primary event in the visual process. Fortunately, there are many experimental constraints that limit drastically the selection of models for this intermediate. These constraints include the following observations: (i) The formation of bathorhodpsin at 30 K takes less than 6 ps.[2] (ii) The quantum yield of this process is very high (0.7), even at 4 K.[3] (iii) The energy of bathorhodpsin is about 35 kcal/mol higher than that of rhodopsin (about 60% of the light energy is stored).[4] (iv) Special resonance Raman (RR) lines appear in the spectrum of bathorhodopsin.[5] (v) Isorhodopsin that includes 9-cis PSBR as a chromophore is converted by light to bathorhodopsin with low quantum yield.[3] (vi) The rate of formation of bathorhodopsin from deuterated rhodopsin is significantly slower than the corresponding rate when the protein is undeuterated.[2] Any detailed molecular model for bathorhodopsin should be capable of *simulating* these experimental facts. Thus, models of the first step

(1) Birge, R. R. *Annu. Rev. Biophys. Bioeng.* **1981**, *10*, 315.
(2) Peters, K.; Applebury, M. L.; Rentzepis, P. M. *Proc. Natl. Acad. Sci. U.S.A.* **1977**, *74*, 3119.
(3) Hurley, J. B.; Ebrey, T. G.; Honig, B.; Ottolenghi, M. *Nature (London)* **1977**, *270*, 540.
(4) Cooper, A. *Nature (London)* **1979**, *282*, 531.
(5) Oseroff, A. R.; Callender, R. H. *Biochemistry* **1974**, *13*, 4243.

0002-7863/82/1504-1469$01.25/0